Nash Equilibrium-based Two-stage Cooperative Operation Strategy for Multi-microgrids Considering Uncertainty

Haiteng Han, Yiteng Xu, Chen Wu, Xiangchen Jiang, Shuyu Cao, Haixiang Zang, Sheng Chen, and Zhinong Wei

***Abstract*—Uncertainties on both the source and demand side pose challenges for the day-to-day management of distributed power systems, such as microgrids (MGs). To harness the potential for flexible scheduling within MGs and to explore the economic and environmental advantages of cooperative interactions between multiple MGs, this paper develops a two-stage power-sharing model for day-ahead and intraday operations across multi-MGs. The intraday stage, which takes into account the prediction errors caused by uncertainty, refines the day-ahead results by factoring in real-time fluctuations in renewable energy sources and loads, changes in equipment status, and the scheduling of various demand response resources. At the end of the intraday optimal scheduling process, the profits from MGs are allocated according to a generalized Nash equilibrium. A case study involving three MGs within a distribution network, examining both island and cooperative operation strategies, demonstrates the practicality and effectiveness of the proposed approach.**

***Index Terms*—Multi-microgrids, two-stage scheduling, Nash equilibrium, Gaussian back substitution-alternating direction multiplier method (GBS-ADMM).**

I. Introduction

The global economy has seen considerable expansion in the 21st century. To address the increasing scarcity of fossil fuels and the environmental issues associated with climate change, nations worldwide have been vigorously advocating for an energy transition. Traditional thermal power generation, which remains the most prevalent source of electricity, faces challenges related to environmental pollution and resource consumption. Consequently, improving the operating efficiency of existing units or advancing the efficient utilization of renewable energy sources (RES) is crucial for the decarbonization and clean development of power systems [1].

Power systems are extensive, and complex, and involve tightly integrated equipment. In contrast, microgrids (MGs), chosen by this paper, with their compact scale, efficiently manage resources within a limited area, enabling flexible scheduling and control, and are thus ideal for integrating new technologies [2]. In [3], a two-stage two-level optimization method has been proposed for multi-carrier energy distribution systems and MG systems, incorporating demand response (DR) in energy trading and assessing system resilience to shocks. Additionally, reference [4] proposed a fault control strategy, alongside a coordinated MG fault detection method, enhancing protection strategies for various MG operation modes. Reference [5] addressed optimizing the power quality of MGs by allowing the formation of minimum output impedance for distributed generators. Moreover, reference [6] introduced the carbon capture system (CCS) and power-to-gas (P2G) in MGs, evaluating the comprehensive benefits and capacity allocation of electro-thermal hybrid shared energy storage. In [7], the authors examined operational efficiency in MGs containing photovoltaic (PV), wind turbines (WT), and combined heat and power (CHP) units. Furthermore, reference [8] included CHP and electric vehicle (EV) in DG, proposing a power sizing strategy integrating sources, storage, and load, and constructed a two-level hybrid energy storage system (ESS) with three types of storage. Additionally, research has explored the topological enhancements and operational control of MGs. Reference [9] elaborated a new strategy based on cooperative game theory models to encourage and manage the interactions in a MG network.

RES are crucial for power system decarbonization [10]. However, their output is highly variable due to numerous influencing factors, leading to operational uncertainties. On the one hand, the uncertainty leads

Received: February 10, 2024
Accepted: July 23, 2024
Published Online: November 1, 2024
Haiteng Han, Yiteng Xu, Chen Wu (corresponding author), Xiangchen Jiang, Shuyu Cao, Haixiang Zang, Sheng Chen, and Zhinong Wei are with the School of Electrical and Power Engineering, Hohai University, Nanjing 211100, China (e-mail: hanht@hhu.edu.cn; xuyt2023@163.com; cwusgcc@gmail.com; 231606030018@hhu.edu.cn; njcsyhhu@outlook.com; zanghaixiang@hhu.edu.cn; chenshenghhu@163.com; wzn_nj@263.net).
DOI: 10.23919/PCMP.2024.000295

to the difficulty of supply and demand forecast, affecting the supply-demand balancing in power markets. On the other hand, the uncertainty may cause operators to reduce investment in RES, which is not conducive to its development and energy trading. MGs are essential for integrating diverse RES into power systems. Reference [11] developed a pool-based DR exchange model in which economic DR is traded among DR participants as an alternative for managing the variability of RES. Reference [12] emphasized the need for inverter-based regulation of RES output, proposing a voltage control strategy graded under voltage limit. Reference [13] presented a robust optimal dispatch method considering the risk of insufficient flexibility in distribution grids. Reference [14] introduced a modified fuzzy logic control topology-based two-degree-of-freedom-tilt derivative controller, ensuring future power system reliability. Most of the existing research focuses on problems within individual systems. However, an individual system has limited capacity to handle uncertainties and often depend on the external grid. Focusing solely on DR to address RES uncertainties can overlook internal load fluctuations and undervalue the regulatory potential of other system components. Existing research has rarely smoothed out uncertainty through the coordinated operation of multiple small systems, or utilizing devices within the system, which is the focus of this paper.

When multiple entities collaborate to participate in the electricity market, it is essential to have reasonable transaction models to balance the diverse interests of all parties. Reference [15] developed a two-level model for the participation of integrated energy service providers (IESP) in the electric-carbon peer-to-peer (P2P) market, where part of the carbon emission responsibility is allocated to the loads. This approach reduces the carbon emission costs for P2P transaction participants and decreases the overall system emissions. Reference [16] employed conditional value-at-risk (CVaR) theory to quantify the potential risks associated with the inherent stochastic nature of RES and proposed a multi-prosumer distributed trading model. Reference [17] proposed a block chain-based multi-level P2P energy trading framework, optimizing distributed energy resources to enhance grid stability and increase the efficiency of RES utilization. The authors in [18] focuses on the classification and in-depth analysis of recent studies that propose game-theoretic approaches for decision optimization of multiple demand users. Stackelberg's game theory based on the P2P transaction model principles was applied to develop a community-integrated energy system model in [19], ensuring fair transaction pricing among prosumers. Additionally, a novel competition padding auction (CPA) mechanism for P2P energy trading is proposed in [20] to address the budget deficit problem while holding the advantages of the widely-used Vickrey-Clarke-Groves mechanism. Current research emphasizes multi-principal day-ahead trading strategies. By emphasizing the need for interoperability among MGs, managing source and demand scheduling at finer time scales, this paper extends the issue of interest in electricity markets to the intraday stage, and gives criteria for the distribution of profits to ensure fairness among stakeholders involved.

This paper constructs a two-stage day-ahead-intraday multi-MGs power-sharing model to explore flexible scheduling opportunities among sources, storage, and load. The day-ahead stage addresses distributed optimization, while the intraday stage incorporates real-time fluctuations of RES and load, equipment statuses, and various DR resources. The model aims to maximize economic benefits and reduce the carbon footprint through cooperative MGs operation. Profit distribution among MGs is determined by Nash equilibrium. This study also considers the temporal and spatial characteristics of DR. The primary contributions are as follows.

1) An alternating direction multiplier method (ADMM) with Gaussian back substitution (GBS) is employed to address the distributed scheduling problem among MGs, with non-dominated sorting genetic algorithm III (NSGA-III) utilized for multi-objective profit distribution. Both algorithms demonstrate robust convergence and identify high-quality solutions.

2) A Nash equilibrium-based energy-sharing method is proposed to enhance cooperative profits and ensure fairness among MGs, incentivizing operators to engage in economically efficient, low-carbon power interactions.

3) A day-ahead-intraday two-stage scheduling model for multi-MGs is developed, enabling complementary operations among MGs with diverse equipment by incorporating temporal dynamics and spatial variability in DR.

The rest of this paper is structured as follows. Section II establishes a two-stage scheduling model for multi-MGs and outlines a corresponding post-cooperation redistribution strategy. Section III introduces solution methodologies and details of the overall solution process. Section IV analyzes a coalition of three selected MGs for a case study, presenting and discussing numerical results. Finally, Section V provides concluding remarks.

II. Optimal Scheduling of Multiple MGs Considering Day-ahead-intraday Stages

This paper investigates CHP MGs, which integrate diverse generating units, equipment, ESS, and loads, operating with synergies across multiple energy types. To enhance economic efficiency, it conducts sequential day-ahead and intraday scheduling, concluding with profit distribution at the end of the intraday stage.

A. Day-ahead Low-carbon Scheduling Model for MGs

The day-ahead scheduling model for low-carbon operations considers both the operational costs of various devices and the power-sharing among MGs. Consequently, the objective function of this stage aims to minimize the system's operating cost C_i^{DA} :

$$C_i^{\mathrm{DA}}=C_i^{\mathrm{DRDA}}+C_i^{\mathrm{ESS}}+C_i^{\mathrm{CO_2}}+C_i^{\mathrm{res}}+C_i^{\mathrm{out}}+C_i^{\mathrm{aba}}+C_i^{\mathrm{ex}}+C_i^{\mathrm{G}} \quad (1)$$

where C_i^{DRDA} represents the DR cost of MGs at the day-ahead stage; C_i^{ESS} denotes the degradation cost of ESS; $C_i^{\mathrm{CO_2}}$ indicates the cost of carbon emissions and trading; C_i^{res} signifies the cost of operation and maintenance (O&M) of RES while C_i^{out} represents the cost of the MG's interaction with outside; C_i^{ada} denotes the cost of the penalty for abandoned RES; C_i^{ex} indicates the transit fee for power-sharing while C_i^{G} stands for the cost of generating units, which varies depending on the type of generating units. The calculation method for each cost is described below.

1) Generating Units Operating Cost

CHP units provide practical solutions for fulfilling both power and heat demands simultaneously. By recovering waste heat during power generation, these units can achieve operational efficiencies of up to 90% and reduce pollutant gas emissions by approximately 13%–18%, thereby integrating functional safety and reliability advantages [21]. In this study, considering the operating constraints of CHP units, a gas furnace (GF) is introduced to augment heat production. The relationship between the power generation of the CHP unit $P_{i,t}^{\mathrm{CHP}}$ and the heat production of the GF at time t $H_{i,t}^{\mathrm{GF}}$, along with gas consumption, are detailed as follows:

$$P_{i,t}^{\mathrm{CHP}}=Q_{\mathrm{C}}V_{i,t}^{\mathrm{CHP}}\eta_{\mathrm{CHP}} \quad (2)$$

$$H_{i,t}^{\mathrm{GF}}=Q_{\mathrm{C}}V_{i,t}^{\mathrm{GF}}\eta_{\mathrm{GF}} \quad (3)$$

where Q_{C} represents the calorific value of natural gas per unit of combustion; $V_{i,t}^{\mathrm{CHP}}$ and $V_{i,t}^{\mathrm{GF}}$ denote the volumes of natural gas consumed by the CHP unit and the GF, respectively; η_{CHP} and η_{GF} indicate the effectiveness of the CHP unit and the GF in generating electricity and heat, respectively.

Therefore, for the MGs set I_1 containing CHP units, the cost of operating the generating units C_i^{G} is:

$$C_i^{\mathrm{G}}=\sum_{t=1}^{T}aP_{i,t}^{\mathrm{CHP}},\ \forall i\in I_1 \quad (4)$$

where a represents the unit generation cost factor for the CHP units.

Notably, power and heat generation in CHP units, i.e., $P_{i,t}^{\mathrm{CHP}}$ and $H_{i,t}^{\mathrm{CHP}}$, are coupled with each other and cannot be controlled separately. Let ω_1 represent the minimum output, ω_2 for normal operation, and ω_3 for maximum output. The thermoelectric coupling constraint of the CHP unit is expressed as:

$$\begin{aligned}&\max\left\{P_{\min}^{\mathrm{CHP}}+\omega_1H_{i,t}^{\mathrm{CHP}},P_{\mathrm{hmin}}^{\mathrm{CHP}}+\omega_2\left(H_{i,t}^{\mathrm{CHP}}-H_{\mathrm{pmin}}^{\mathrm{CHP}}\right)\right\}\leqslant\\&P_{i,t}^{\mathrm{CHP}}\leqslant P_{\max}^{\mathrm{CHP}}+\omega_3H_{i,t}^{\mathrm{CHP}}\end{aligned} \quad (5)$$

where $P_{\min}^{\mathrm{CHP}}$ and $P_{\max}^{\mathrm{CHP}}$ are the lower and upper limits of output when the CHP unit is only generating power, respectively; $P_{\mathrm{hmin}}^{\mathrm{CHP}}$ is the minimum output of the CHP unit when producing heat; and $H_{\mathrm{pmin}}^{\mathrm{CHP}}$ is the heat production of the CHP unit at minimum output.

The aforementioned equation delineates the characteristics of the power supply from a CHP unit as influenced by its heating output.

Both the CHP unit and the GF are required to comply with the appropriate operational constraints simultaneously:

$$\begin{cases}P_{i,\min}^{\mathrm{CHP}}\leqslant P_{i,t}^{\mathrm{CHP}}\leqslant P_{i,\max}^{\mathrm{CHP}}\\H_{i,\min}^{\mathrm{CHP}}\leqslant H_{i,t}^{\mathrm{CHP}}\leqslant H_{i,\max}^{\mathrm{CHP}}\\H_{i,\min}^{\mathrm{GF}}\leqslant H_{i,t}^{\mathrm{GF}}\leqslant H_{i,\max}^{\mathrm{GF}}\end{cases} \quad (6)$$

where $P_{i,\max}^{\mathrm{CHP}}$ and $P_{i,\min}^{\mathrm{CHP}}$ represent the upper and lower output limits of the CHP unit, respectively; $H_{i,\max}^{\mathrm{CHP}}$ and $H_{i,\min}^{\mathrm{CHP}}$ denote the upper and lower heating limits of the CHP unit, respectively; $H_{i,\max}^{\mathrm{GF}}$ and $H_{i,\min}^{\mathrm{GF}}$ indicate the upper and lower limits of GF, respectively.

By adjusting the rate of steam extraction, carbon capture plants can modify their output more quickly than conventional thermal power plants, which require changing the boiler's operating state 0. For shorter time scales of RES and load forecasting in the intraday stage, carbon capture plants can handle PV and WT output curtailment and load loss due to their faster net output adjustment capability.

In this paper, the carbon emissions from carbon capture power plants are modeled as follows:

$$E_{i,t}^{\mathrm{gen}}=P_{i,t}^{\mathrm{gen}}\alpha_i^{\mathrm{gen}}-E_{i,t}^{\mathrm{ccs}} \quad (7)$$

$$E_{i,t}^{\mathrm{ccs}}=\eta_{\mathrm{ccs}}P_{i,t}^{\mathrm{gen}}\alpha_i^{\mathrm{gen}}\gamma_{i,t} \quad (8)$$

where $E_{i,t}^{\mathrm{gen}}$ represents the actual carbon emissions; $P_{i,t}^{\mathrm{gen}}$ denotes the total output; α_i^{gen} indicates the carbon intensity of the unit; $E_{i,t}^{\mathrm{ccs}}$ signifies the amount of carbon capture; η_{ccs} and $\gamma_{i,t}$ are the efficiency and flue gas split ratio, respectively.

Accordingly, the power consumption for carbon capture $P_{i,t}^{\mathrm{ccs}}$ is defined as:

$$P_{i,t}^{\mathrm{ccs}}=\beta_{\mathrm{ccs}}E_{i,t}^{\mathrm{ccs}} \quad (9)$$

where β_{ccs} represents the power consumption per unit weight of carbon capture.

The total output $P_{i,t}^{\mathrm{gen}}$ is the sum of net power output $P_{i,t}^{\mathrm{e}}$, the power used for carbon capture $P_{i,t}^{\mathrm{ccs}}$, and a fixed power consumption P_i^0:

$$P_{i,t}^{\text{gen}} = P_{i,t}^{\text{e}} + P_{i,t}^{\text{ccs}} + P_i^0 \tag{10}$$

For the MGs set I_2, which includes the carbon capture plant, the operating cost C_i^{G} is:

$$C_i^{\text{G}} = \sum_{t=1}^{T} b(P_{i,t}^{\text{gen}})^2 + cP_{i,t}^{\text{gen}} + d + eP_{i,t}^{\text{ccs}},\ \forall i \in I_2 \tag{11}$$

where b, c, d, and e are the corresponding cost factors.

Power coordination between net output and carbon capture is managed by adjusting the flue gas split ratio. The following constraints must be satisfied for the operation of a carbon capture power plant:

$$x_{i,t}^{\text{gen}} P_{i,\min}^{\text{gen}} \leqslant P_{i,t}^{\text{gen}} \leqslant x_{i,t}^{\text{gen}} P_{i,\max}^{\text{gen}} \tag{12}$$

$$0 \leqslant E_{i,t}^{\text{ccs}} \leqslant \eta_{\text{ccs}} P_{i,\max}^{\text{gen}} \alpha_i^{\text{gen}} \gamma_{i,\max} \tag{13}$$

where $P_{i,\max}^{\text{gen}}$ and $P_{i,\min}^{\text{gen}}$ represent the upper and lower output limits; $x_{i,t}^{\text{gen}}$ denotes the unit start-stop status, taking 0 for stopping, and 1 for running; and $\gamma_{i,\max}$ indicates the upper limit of the flue gas split ratio.

This establishes the range constraint for the net output of carbon capture power plants:

$$P_{i,\min}^{\text{gen}} - \eta_{\text{ccs}} P_{i,\min}^{\text{gen}} \alpha_i^{\text{gen}} \gamma_{i,\max} - P_i^0 \leqslant P_{i,t}^{\text{e}} \leqslant P_{i,\max}^{\text{gen}} - P_i^0 \tag{14}$$

Additionally, carbon capture power plants must operate within their ramping constraints;

$$R_{\text{d}} \leqslant \left| P_{i,t}^{\text{gen}} - P_{i,t-1}^{\text{gen}} \right| \leqslant R_{\text{u}} \tag{15}$$

where R_{u} and R_{d} represent the upward and downward ramping rates of the unit, respectively.

2) DR Cost

The loads in this paper are categorized as rigid and flexible, with flexible loads participating in DR. DR is further classified into price-based demand response (PDR) and incentive-based demand response (IDR). IDR can align the load profile to match the output of units with varying carbon intensities, thus reducing carbon emissions [23]. PDR can schedule load increases during low-demand periods to utilize RES and decrease load during peak times to reduce the output from high-carbon units [24]. Considering the response time, IDR resources are divided into two classes. Class A IDR has a response time of about one hour, with the scheduling plan determined in the day-ahead stage. Class B IDR, with a response time of 5–15 min, is scheduled in the intraday stage.

Based on this, the power load $P_{i,t}^{\text{L}}$ in this paper consists of the transferable load $P_{i,t}^{\text{tran}}$, the cuttable load $P_{i,t}^{\text{cut}}$, and the rigid load $P_{i,t}^{\text{fix}}$:

$$P_{i,t}^{\text{L}} = P_{i,t}^{\text{fix}} + P_{i,t}^{\text{tran}} + P_{i,t}^{\text{cut}} \tag{16}$$

Similarly, the heat load $H_{i,t}^{\text{L}}$ includes the cuttable load $H_{i,t}^{\text{cut}}$ and the rigid load $H_{i,t}^{\text{fix}}$:

$$H_{i,t}^{\text{L}} = H_{i,t}^{\text{fix}} + H_{i,t}^{\text{cut}} \tag{17}$$

Therefore, the DR cost for the day-ahead stage is:

$$C_i^{\text{DRDA}} = \sum_{t=1}^{T} \pi^{\text{ptran}} P_{i,t}^{\text{tran}} + \pi^{\text{pDRA}} P_{i,t}^{\text{DRA}} + \pi^{\text{hcut}} H_{i,t}^{\text{cut}} \tag{18}$$

where $P_{i,t}^{\text{DRA}}$ represents the amount of Class A IDR participating in the dispatch, in which $P_{i,t}^{\text{DRA}} = P_{i,t}^{\text{cut}}$; π^{ptran}, π^{pDRA} and π^{hcut} denote the cost of compensating for the power per unit corresponding to different DR, respectively.

The following constraints apply to cuttable and transferable loads:

$$\delta^{\text{pcut}} P_{i,t}^{\text{fix}} \leqslant P_{i,t}^{\text{cut}} \leqslant 0,\ \forall t \in T_{\text{cut}},\ \forall i \in I_{\text{cut}} \tag{19}$$

$$-\delta^{\text{ptran}} P_{i,t}^{\text{fix}} \leqslant P_{i,t}^{\text{tran}} \leqslant \delta^{\text{ptran}} P_{i,t}^{\text{fix}} \tag{20}$$

$$\sum_{t=1}^{T} P_{i,t}^{\text{tran}} \Delta t = 0 \tag{21}$$

where $\delta^{\text{pcut}} \in [-1,0]$ and $\delta^{\text{ptran}} \in [0,1]$ denote the proportionality factors of the cuttable and transferable power loads, respectively; while Δt indicates the time interval; T_{cut} and I_{cut} denote the set of periods and MGs where DR is permissible. Equations (19) and (20) impose the upper and lower bounds for DR, while Eq. (21) ensures that the total transferable power load within a dispatch interval is zero.

For heat loads, only the constraints on cuttable loads are considered:

$$\delta^{\text{hcut}} H_{i,t}^{\text{fix}} \leqslant H_{i,t}^{\text{cut}} \leqslant 0 \tag{22}$$

where $\delta^{\text{hcut}} \in [-1,0]$ represents the proportionality factor for the cuttable heat load.

3) ESS Degradation Cost

In the MG model proposed in this paper, the state of charge $S_{i,t}^{\text{SOC}}$ of ESS at time t is described as follows:

$$\begin{cases} S_{i,t}^{\text{SOC}} = S_{i,t-1}^{\text{SOC}} \eta_{\text{loss}} + \eta_{\text{ch}} P_{i,t}^{\text{ch}} - \dfrac{P_{i,t}^{\text{disc}}}{\eta_{\text{disc}}} \\ S_{i,\min}^{\text{SOC}} \leqslant S_{i,t}^{\text{SOC}} \leqslant S_{i,\max}^{\text{SOC}} \\ S_{i,\text{end}}^{\text{SOC}} = S_{i,0}^{\text{SOC}} \\ 0 \leqslant P_{i,t}^{\text{ch}} \leqslant x_{i,t}^{\text{ch}} P_{i,\max}^{\text{ch}} \\ 0 \leqslant P_{i,t}^{\text{disc}} \leqslant x_{i,t}^{\text{disc}} P_{i,\max}^{\text{disc}} \\ x_{i,t}^{\text{ch}} \leqslant x_{i,t}^{\text{disc}} \leqslant 1 \end{cases} \tag{23}$$

where η_{loss} denotes the self-loss factor of ESS; η_{ch} and η_{disc} are the charging and discharging efficiencies, respectively; $P_{i,t}^{\text{ch}}$ and $P_{i,t}^{\text{disc}}$ represent the charging and discharging power, respectively; $S_{i,\max}^{\text{SOC}}$ and $S_{i,\min}^{\text{SOC}}$ are the upper and lower limits of ESS, respectively; $P_{i,\max}^{\text{ch}}$ and

$P_{i,\max}^{\text{disc}}$ are the upper charging power limits, respectively; while $x_{i,t}^{\text{ch}}$ and $x_{i,t}^{\text{disc}}$ are binary charging and discharging state variables. Notably, $x_{i,t}^{\text{ch}}=1$ and $x_{i,t}^{\text{disc}}=0$ for charging while $x_{i,t}^{\text{ch}}=0$ and $x_{i,t}^{\text{disc}}=1$ for discharging. Equation (23) specifies the conservation of charge between the initial and final phases, and stipulates that the ESS cannot charge and discharge simultaneously.

On this basis, the degradation cost of ESS can be expressed as:

$$C_i^{\text{ESS}}=\sum_{t=1}^{T}\pi^{\text{ESS}}(P_{i,t}^{\text{ch}}+P_{i,t}^{\text{disc}}) \tag{24}$$

where π^{ESS} represents unit charge/discharge loss cost.

4) Carbon Emissions and Trading Cost

Given that MGs may purchase power from external grids, it is crucial to account for the carbon emissions associated with this part when calculating the carbon emissions of the MG. For MGs with various devices, their carbon emissions $E_i^{\text{CO}_2}$ can be expressed as follows:

$$\begin{cases} E_i^{\text{CO}_2}=\sum_{t=1}^{T}\alpha_i^{\text{CHP}}(P_{i,t}^{\text{CHP}}+\omega_1 H_{i,t}^{\text{CHP}})+ \\ \qquad \alpha_i^{\text{GF}}H_{i,t}^{\text{GF}}+\alpha_i^{\text{buy}}P_{i,t}^{\text{buy}},\ \forall i\in I_1 \\ E_i^{\text{CO}_2}=\sum_{t=1}^{T}E_{i,t}^{\text{gen}}+\alpha_i^{\text{buy}}P_{i,t}^{\text{buy}},\ \forall i\in I_2 \end{cases} \tag{25}$$

where $P_{i,t}^{\text{buy}}$ represents the power purchased from the upper grid; a_i^{CHP} and a_i^{GF} denote the carbon emission factors of the CHP units and GF, respectively [25]; and a_i^{buy} indicates the carbon emission factor for the power purchase behavior.

The carbon allowance $D_i^{\text{CO}_2}$ for MG*i* can be expressed as follows:

$$\begin{cases} D_i^{\text{CO}_2}=\sum_{t=1}^{T}A_i^{\text{CHP}}P_{i,t}^{\text{CHP}}+A_i^{\text{res}}P_{i,t}^{\text{res}},\ \forall i\in I_1 \\ D_i^{\text{CO}_2}=\sum_{t=1}^{T}A_i^{\text{gen}}P_{i,t}^{\text{gen}}+A_i^{\text{res}}P_{i,t}^{\text{res}},\ \forall i\in I_2 \end{cases} \tag{26}$$

where $P_{i,t}^{\text{res}}$ represents the actual RES consumed by the MG*i*, including PV and WT; A_i^{CHP}, A_i^{gen}, and A_i^{res} denote the carbon quota for the CHP unit, carbon capture plant, and RES, respectively.

Carbon emissions and trading cost is given by the following equation:

$$C_i^{\text{CO}_2}=\pi^{\text{CO}_2}(E_i^{\text{CO}_2}-D_i^{\text{CO}_2}) \tag{27}$$

where π^{CO_2} denotes the unit carbon transaction cost factor.

5) RES O&M Cost and Penalty Cost

MGs incorporating RES must consider O&M cost inherent with their daily operation:

$$C_i^{\text{res}}=\sum_{t=1}^{T}\pi^{\text{res}}P_{i,t}^{\text{res}} \tag{28}$$

where π^{res} represents the O&M costs factor per unit of RES.

To encourage MGs to maximize RES utilization, a penalty cost for RES abandonment is established:

$$C_i^{\text{aba}}=\sum_{t=1}^{T}\pi^{\text{aba}}(P_{i,t}^{\text{WTDA}}+P_{i,t}^{\text{PVDA}}-P_{i,t}^{\text{res}}) \tag{29}$$

where $P_{i,t}^{\text{WTDA}}$ and $P_{i,t}^{\text{PVDA}}$ represent the output of WT and PV in the day-ahead stage, respectively; and π^{aba} denotes the unit penalty cost factor.

6) MG External Cost

MGs may incur expenses related to purchasing or selling power, as well as acquiring natural gas:

$$C_i^{\text{out}}=\sum_{t=1}^{T}\pi^{\text{gas}}(V_{i,t}^{\text{CHP}}+V_{i,t}^{\text{GF}})+\pi_t^{\text{buy}}P_{i,t}^{\text{buy}}-\pi_t^{\text{sell}}P_{i,t}^{\text{sell}} \tag{30}$$

where $P_{i,t}^{\text{sell}}$ represents the power sold by MG to upper grid; π^{gas} denotes the cost per volume of gas purchased; π_t^{buy} and π_t^{sell} are the prices of power purchased and sold by MG, respectively.

Given the unit power over grid cost π^{ex}, the interaction cost due to transmission between MG is:

$$C_i^{\text{ex}}=\sum_{t=1}^{T}\pi^{\text{ex}}\left|P_{ij,t}\right| \tag{31}$$

where $P_{ij,t}$ represents the power transmitted from MG*i* to MG*j*.

7) System Operation Constraints

In addition to the specific constraints imposed on individual equipment types, MGs must ensure overall power balance and backup adequacy during operation. Considering power interactions between MGs, they must satisfy their respective power and heat balance constraints:

$$\begin{cases} P_{i,t}^{\text{res}}+P_{i,t}^{\text{CHP}}+P_{i,t}^{\text{disc}}+P_{i,t}^{\text{buy}}=P_{i,t}^{\text{L}}+P_{i,t}^{\text{ch}}+P_{i,t}^{\text{sell}}+P_{ij,t},\ \forall i\in I_1 \\ P_{i,t}^{\text{res}}+P_{i,t}^{\text{e}}+P_{i,t}^{\text{disc}}+P_{i,t}^{\text{buy}}=P_{i,t}^{\text{L}}+P_{i,t}^{\text{ch}}+P_{i,t}^{\text{sell}}+P_{ij,t},\ \forall i\in I_2 \end{cases} \tag{32}$$

$$H_{i,t}^{\text{CHP}}+H_{i,t}^{\text{GF}}=H_{i,t}^{\text{L}} \tag{33}$$

Power trading between MGs and the upper grid adheres to the following constraints:

$$\begin{cases} 0\leqslant P_{i,t}^{\text{buy}}\leqslant x_{i,t}^{\text{buy}}P_{i,\max}^{\text{buy}} \\ 0\leqslant P_{i,t}^{\text{sell}}\leqslant x_{i,t}^{\text{sell}}P_{i,\max}^{\text{sell}} \\ x_{i,t}^{\text{buy}}+x_{i,t}^{\text{sell}}\leqslant 1 \end{cases} \tag{34}$$

where $x_{i,t}^{\text{buy}}$ and $x_{i,t}^{\text{sell}}$ are binary variables indicating buying and selling states, $P_{i,\max}^{\text{buy}}$ and $P_{i,\max}^{\text{sell}}$ are the maximum limits for purchased and sold power, respectively. Equation (34) ensures that MG cannot simultaneously purchase and sell power.

Furthermore, the transmitted power at any time period must adhere to the safety constraint limit $P_{ij,\max}$ of the contact line:

$$\left|P_{ij,t}\right| \leqslant P_{ij,\max} \tag{35}$$

Systems incorporating carbon capture power plants must adhere to spinning reserve constraints:

$$\begin{cases} \min\left\{R_{\text{u}}, P_{i,\max}^{\text{gen}} - P_{i,t}^{\text{gen}}\right\} \geqslant s_{\text{u}} P_{i,t}^{\text{L}} \\ \min\left\{R_{\text{d}}, P_{i,t}^{\text{gen}} - P_{i,\min}^{\text{gen}}\right\} \geqslant s_{\text{d}} P_{i,t}^{\text{L}} \end{cases} \quad \forall i \in I_2 \tag{36}$$

where s_{u} and s_{d} denote the upper and lower rotating reserve capacity factors required for the system, respectively.

B. Intraday Power Interaction Model for MG

1) Intraday Dispatch Objective Function

The objective function of the intraday scheduling stage aims to minimize the operational cost C_i^{ID}, considering the scheduling plan of Class A IDR and the associated costs of Class B IDR. This stage needs to consider forecast errors of RES and load due to uncertainty, as well as the corresponding O&M and penalty cost. Moreover, the time scale of system scheduling needs to be changed. Therefore the objective function of the intraday stage is:

$$\begin{cases} C_i^{\text{ID}} = C_i^{\text{DRID}} + C_i^{\text{ESS}} + C_i^{\text{CO}_2} + C_i^{\text{res}} + C_i^{\text{out}} + C_i^{\text{aba}} + C_i^{\text{ex}} + C_i^{\text{G}} \\ C_i^{\text{DRID}} = C_i^{\text{DRDA}} + \sum_{t=1}^{T} \pi^{\text{pDRB}} P_{i,t}^{\text{DRB}} \\ C_i^{\text{aba}} = \sum_{t=1}^{T} \pi^{\text{aba}} \left(P_{i,t}^{\text{WTID}} + P_{i,t}^{\text{PVID}} - P_{i,t}^{\text{res}}\right) \end{cases} \tag{37}$$

where C_i^{DRID} represents the DR cost; $P_{i,t}^{\text{DRB}}$ denotes the class B IDR participating in intraday dispatch; π^{pDRB} indicates the corresponding unit power compensation cost; $P_{i,t}^{\text{PVID}}$ signifies the actual PV output in the intraday stage; while $P_{i,t}^{\text{WTID}}$ is the actual WT output in the intraday stage.

WT can adjust their output through pitch angle and rotor speed control [26], but actual output deviates from the predicted value [27]. The variability in WT output is modeled as an uncertain variable ε_{W}. Consequently, the WT output must adhere to the following boundary and climb constraints:

$$P_{i,t}^{\text{WT}} = P_{i,t}^{\text{WTDA}} + \varepsilon_{\text{W}} \tag{38}$$

$$0 \leqslant P_{i,t}^{\text{WT}} \leqslant P_{i,\max}^{\text{WT}} \tag{39}$$

$$R_{\text{d}}^{\text{WT}} \leqslant \left|P_{i,t}^{\text{WT}} - P_{i,t-1}^{\text{WT}}\right| \leqslant P_{\text{u}}^{\text{WT}} \tag{40}$$

where $P_{i,\max}^{\text{WT}}$ represents the upper limit of WT output; while R_{u}^{WT} and R_{d}^{WT} denote the maximum upward and downward ramping rates, respectively.

During the intraday stage, adjustments are necessary for ramping constraints, spinning reserve constraints, as well as power and heat load balance constraints for units.

$$\begin{cases} R_{\text{dID}} \leqslant \left|P_{i,t}^{\text{gen}} - P_{i,t-1}^{\text{gen}}\right| \leqslant R_{\text{uID}} \\ \min\left\{R_{\text{uID}}, P_{i,\max}^{\text{gen}} - P_{i,t}^{\text{gen}}\right\} \geqslant s_{\text{u}} P_{i,t}^{\text{L}} \\ \min\left\{R_{\text{dID}}, P_{i,t}^{\text{gen}} - P_{i,\min}^{\text{gen}}\right\} \geqslant s_{\text{d}} P_{i,t}^{\text{L}} \\ P_{i,t}^{\text{LID}} = P_{i,t}^{\text{fixID}} + P_{i,t}^{\text{tran}} + P_{i,t}^{\text{DRA}} + P_{i,t}^{\text{DRB}} \\ H_{i,t}^{\text{LID}} = H_{i,t}^{\text{fixID}} + H_{i,t}^{\text{cutID}} \\ \delta^{\text{pcut}} P_{i,t}^{\text{fixID}} \leqslant P_{i,t}^{\text{DRA}} \leqslant 0, \quad \forall t \in T_{\text{cut}}, \forall i \in I_{\text{cut}} \\ \delta^{\text{pcutID}} P_{i,t}^{\text{fixID}} \leqslant P_{i,t}^{\text{DRB}} \leqslant 0, \quad \forall t \in T_{\text{cut}}, \forall i \in I_{\text{cut}} \\ -\delta^{\text{ptran}} P_{i,t}^{\text{fixID}} \leqslant P_{i,t}^{\text{tran}} \leqslant \delta^{\text{ptran}} P_{i,t}^{\text{fixID}} \\ \delta^{\text{hcut}} H_{i,t}^{\text{fixID}} \leqslant H_{i,t}^{\text{cutID}} \leqslant 0 \end{cases} \tag{41}$$

where R_{uID} and R_{dID} represent the upward and downward ramping rates of thermal units in intraday time scale, respectively; $P_{i,t}^{\text{fixID}}$, $H_{i,t}^{\text{fixID}}$, $P_{i,t}^{\text{LID}}$ and $H_{i,t}^{\text{LID}}$ denote the actual load before and after DR, respectively; $\delta^{\text{pcutID}} \in [-1,0]$ denotes the proportionality factors of the cuttable power loads in the intraday stage. The equation above establishes constraints on the upper and lower limits of DR.

Similarly, the intraday stage must adhere to energy balance constraints:

$$\begin{cases} P_{i,t}^{\text{res}} + P_{i,t}^{\text{CHP}} + P_{i,t}^{\text{disc}} + P_{i,t}^{\text{buy}} = P_{i,t}^{\text{LID}} + P_{i,t}^{\text{ch}} + P_{i,t}^{\text{sell}} + P_{ij,t}, \ \forall i \in I_1 \\ P_{i,t}^{\text{res}} + P_{i,t}^{\text{e}} + P_{i,t}^{\text{disc}} + P_{i,t}^{\text{buy}} = P_{i,t}^{\text{LID}} + P_{i,t}^{\text{ch}} + P_{i,t}^{\text{sell}} + P_{ij,t}, \ \forall i \in I_2 \end{cases} \tag{42}$$

$$H_{i,t}^{\text{CHP}} + H_{i,t}^{\text{GF}} = H_{i,t}^{\text{LID}} \tag{43}$$

2) Profit Distribution Objective Function

The profits from the daily operation of MG result from revenue earned by the serving users minus operating costs. At the conclusion of the intraday dispatch stage, any reduction in operating costs represents additional profit. This surplus profit must be fairly distributed among MGs, guided by the following three principles in this paper.

1) Profit distribution should consider peak-valley-parity tariffs, ensuring that MGs delivering during peak tariff

periods receive more profit, while those delivering power during low-tariff periods receive less profit.

2) MGs participating in power-sharing should also participate in profit distribution. MGs prioritizing output power should receive higher revenue shares compared to MGs prioritizing power reception.

3) MGs participating in power interaction should not receive less profit after redistribution than they would if operated independently.

Based on this foundation, this paper utilizes generalized Nash equilibrium to simulate the process of profit distribution facilitated by power trading between MGs, establishing a corresponding profit distribution model. Assuming each MG is aware of the bidding strategies of others, no MG can enhance its profit by altering its strategy. this ensures that all MGs achieve a Nash equilibrium state where they cannot decrease their profitability regardless of the trading tariffs set by other MGs, thereby ensuring fairness and credibility in profit distribution. Therefore, the objective function aims to maximize the profit distributed to each MG:

$$f_i = \left(C_i^0 - C_i^{\mathrm{ID}} + \sum_{j \neq i}^{I} \sum_{t=1}^{T} \pi_{ij}^{\mathrm{P2P}} P_{ij,t} \right)^{W_i} \tag{44}$$

where C_i^0 and C_i^{ID} denote the operating costs during independent operation and intraday stage, respectively; $P_{ij,t}$ is determined by solving the scheduling model; π_{ij}^{P2P} is the trading tariff, which results in a total of $(n^2 - n)/2$ variables for a group consisting of n MGs; the weight factor W_i is set by considering the contribution of each MG. Based on the natural pairwise quantitative weight parameter [29], the contribution of individual MG to the MG group can be effectively amplified, allowing each MG to exert corresponding influence in the game. W_i is derived from the following equation:

$$W_i = \mathrm{e}^{\left(\frac{P_i^{\mathrm{EX}}}{\max\left\{P_i^{\mathrm{EX}} \middle| i \in I\right\}} - \frac{\pi_t^{\mathrm{sell}} P_i^{\mathrm{IN}}}{\pi_t^{\mathrm{buy}} \max\left\{P_i^{\mathrm{IN}} \middle| i \in I\right\}} \right)} \tag{45}$$

$$\begin{cases} P_i^{\mathrm{EX}} = \sum_{t=1}^{T} \left| \min\left\{0, P_{ij,t}\right\} \right| \\ P_i^{\mathrm{IN}} = \sum_{t=1}^{T} \left| \max\left\{0, P_{ij,t}\right\} \right| \end{cases} \tag{46}$$

where P_i^{EX} and P_i^{IN} denote the net outflow and inflow power of MG, respectively. Moreover, equation (45) specifies that all MGs participating in power-sharing will receive the corresponding weights, and the one with more output power will be given a higher weight.

When equation (47) is satisfied, MG will participate in profit distribution:

$$C_i^0 - C_i^{\mathrm{ID}} \geqslant -\sum_{j \neq i}^{I} \sum_{t=1}^{T} \pi_{ij}^{\mathrm{P2P}} P_{ij,t} \tag{47}$$

Additionally, the tariff constraints and profit distribution constraints are:

$$\delta_1^{\mathrm{P2P}} \pi_t^{\mathrm{buy}} \leqslant \pi_{ij}^{\mathrm{P2P}} \leqslant \delta_2^{\mathrm{P2P}} \pi_t^{\mathrm{buy}} \tag{48}$$

$$\sum_{i}^{I} \sum_{j \neq i}^{I} \sum_{t=1}^{T} \pi_{ij}^{\mathrm{P2P}} P_{ij,t} = 0 \tag{49}$$

where δ_1^{P2P} and δ_2^{P2P} denote the factors controlling the tariffs for trading, respectively, and equation (49) ensures that the total profit is constant before and after the distribution.

III. Solving Algorithms

A. Overall Solution Procedure

The two-stage scheduling model for MG aims to achieve optimal scheduling of MG in the day-ahead and the intraday stage sequentially. Moreover, profit redistribution is necessary after the intraday scheduling process. To address this, the day-ahead scheduling model needs to be built based on day-ahead data and constraints. Subsequently, the model is solved by the ADMM.

$$\begin{cases} \min \sum_{i=1}^{I} C_i^{\mathrm{DA}}, \ \forall i \in I \\ \text{s.t. } (1) - (36) \end{cases} \tag{50}$$

where I is the set of all MGs.

The intraday stage necessitates additional consideration of equipment constraints, involvement of different types of DR resources, rapid changes in components, such as short-term RES, and fluctuations in load. Then we can construct the following model:

$$\begin{cases} \min \sum_{i=1}^{I} C_i^{\mathrm{ID}}, \ \forall i \in I \\ \text{s.t. } (2) - (14), (18), (21) \\ \text{s.t. } (23) - (28), (30), (31) \\ \text{s.t. } (34), (35), (37) - (43) \end{cases} \tag{51}$$

Given the complexity of the intraday stage is more compared to the day-ahead model, it is solved using GBS-contained ADMM (GBS-ADMM).

After completing the intraday scheduling, the profit needs to be distributed to ensure that the scheduling is reasonable and fair:

$$\begin{cases} \max f_i, \ \forall i \in I \\ \text{s.t. } (44) - (49) \end{cases} \tag{52}$$

Since maximizing the distributed profit of each MG is a multi-objective optimization problem, it can be solved using the NSGA-III algorithm [30].

The overall solution procedure of this paper is shown in the Fig.1.

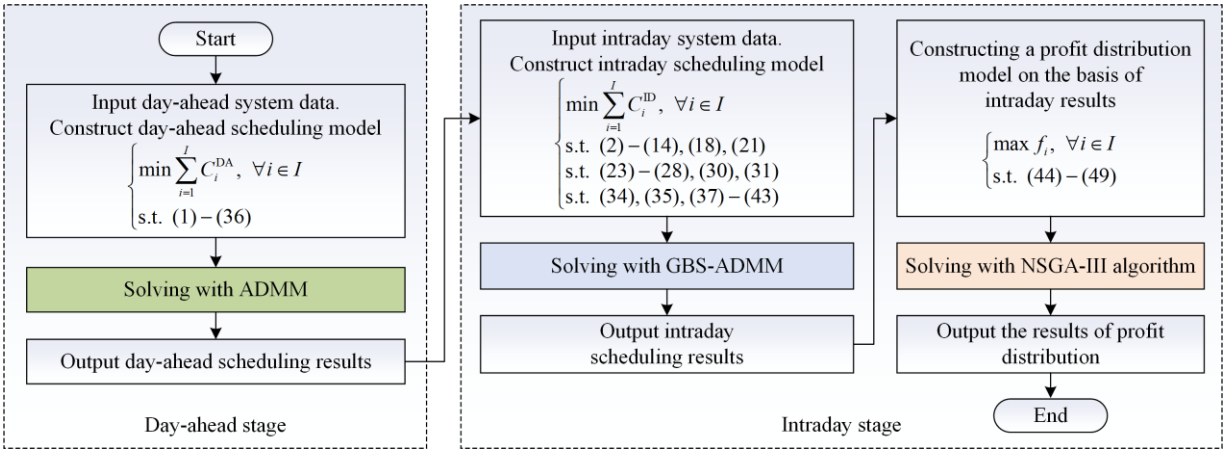

Fig. 1. Overall solution procedure.

B. Solving Optimal Scheduling Problems Based on GBS-ADMM

ADMM is recognized as highly efficient for solving convex optimization problems involving two separable operators [32]. When applying a generalized ADMM to solve the multi-MGs scheduling models (50) and (51) developed in this study, the introduction of an auxiliary variable $P_{ji,t}$ is essential. This variable, in conjunction with the original variable $P_{ij,t}$, facilitates problem decomposition across the three MGs, ensuring compliance with the following constraints:

$$P_{ij,t} + P_{ji,t} = 0 \tag{53}$$

Adding the multiplication factor ρ and the Lagrange multiplier λ, the Lagrangian function $L_i(i=1,2,3)$ is constructed on the basis of the original objective function $C_i(i=1,2,3)$:

Constructing the augmented Lagrangian function:

$$\begin{cases} L_1 = C_1 + \sum_{j\neq 1}^{I}\sum_{t=1}^{T} \lambda_{1j}(P_{1j,t}+P_{j1,t}) + \sum_{j\neq 1}^{I}\sum_{t=1}^{T} \frac{\rho}{2}\left\|P_{1j,t}+P_{j1,t}\right\|_2^2 \\ L_2 = C_2 + \sum_{j\neq 2}^{I}\sum_{t=1}^{T} \lambda_{2j}(P_{2j,t}+P_{j2,t}) + \sum_{j\neq 2}^{I}\sum_{t=1}^{T} \frac{\rho}{2}\left\|P_{2j,t}+P_{j2,t}\right\|_2^2 \\ L_3 = C_3 + \sum_{j\neq 3}^{I}\sum_{t=1}^{T} \lambda_{3j}(P_{3j,t}+P_{j3,t}) + \sum_{j\neq 3}^{I}\sum_{t=1}^{T} \frac{\rho}{2}\left\|P_{3j,t}+P_{j3,t}\right\|_2^2 \end{cases} \tag{54}$$

Assuming the iteration at step $(k+1)$th is ongoing, the decision variables $P_{ij,t}$ corresponding to the other two MGs are fixed, the $P_{ij,t}$ of the current MG is updated, and λ is updated after the completion of the $(k+1)$th iteration. The procedure can be outlined as follows:

$$\begin{cases} P_{1j}^{k+1} = \arg\min L_1(P_{1j}, P_{2j}^{k}, P_{3j}^{k}, \lambda^k) \\ P_{2j}^{k+1} = \arg\min L_2(P_{1j}^{k+1}, P_{2j}, P_{3j}^{k}, \lambda^k) \\ P_{3j}^{k+1} = \arg\min L_3(P_{1j}^{k+1}, P_{2j}^{k+1}, P_{3j}, \lambda^k) \\ \lambda_{ij}^{k+1} = \lambda_{ij}^{k+1}\rho(P_{ij,t}+P_{ji,t}) \end{cases} \tag{55}$$

When dealing with the problem involving three MGs, equation (54) generates six multipliers λ, and according to (55), half of these multipliers will have identical values. To simplify the computation, and prepare for the GBS process later, these multipliers are combined into Lagrange multipliers for the mutual coupling of MGs:

$$\begin{cases} \lambda_1^{k+1} = \lambda_1^{k} + \rho(P_{12,t} + P_{21,t}) \\ \lambda_2^{k+1} = \lambda_2^{k} + \rho(P_{13,t} + P_{31,t}) \\ \lambda_3^{k+1} = \lambda_3^{k} + \rho(P_{23,t} + P_{32,t}) \end{cases} \tag{56}$$

The method above reduces the number of λ by half, thus lowering computational complexity and enhancing efficiency.

At the $(k+1)$th iteration according to (55), P_{1j}^{k+1} is derived from P_{2j}^{k}, P_{3j}^{k}, and λ^k; while P_{2j}^{k+1} is derived from P_{1j}^{k+1}, P_{3j}^{k}, and λ^k; and P_{3j}^{k+1} is derived from P_{1j}^{k+1}, P_{2j}^{k+1}, and λ^k. For the core variable P_{2j}, information from P_{1j}^{k+1} has been utilized in the $(k+1)$ th solution as per (55), while the variable of the kth iteration has been used for P_{3j}^{k}, and similarly for P_{3j}. This creates an unfair information situation. Equation (54) involves six coupled variables grouped into three, incorporating multiple couplings of different operational and equilibrium constraints in the model. Direct extension of ADMM may lead to non-convergence, so the variables in the information imbalance are appropriately complemented. After updating λ, a GBS process is applied the necessary corrections:

$$\begin{bmatrix} P_{21,t}^{k+1} \\ P_{23,t}^{k+1} \\ P_{31,t}^{k+1} \\ P_{32,t}^{k+1} \end{bmatrix} = \begin{bmatrix} P_{21,t}^{k} \\ P_{23,t}^{k} \\ P_{31,t}^{k} \\ P_{32,t}^{k} \end{bmatrix} - \mu \begin{bmatrix} I & -I & 0 & 0 \\ 0 & I & 0 & 0 \\ 0 & 0 & I & -I \\ 0 & 0 & 0 & I \end{bmatrix} \begin{bmatrix} P_{21,t}^{k} - P_{21,t}^{k+1} \\ P_{23,t}^{k} - P_{23,t}^{k+1} \\ P_{31,t}^{k} - P_{31,t}^{k+1} \\ P_{32,t}^{k} - P_{32,t}^{k+1} \end{bmatrix} \tag{57}$$

where a suitably small amount $\mu \in [0.9, 0.95]$ is the correction factor for GBS. This ensures the convergence of the algorithm [28].

Following the GBS process, it is necessary to calculate the original residuals and dual residuals to determine the convergence status of the iterations.

$$\begin{cases} r_{\mathrm{o}} = \sum_{j\neq i}^{I}\sum_{t=1}^{T}\left\|P_{ij,t}^{k+1} - P_{ji,t}^{k+1}\right\|_2 \leqslant \varepsilon_{\mathrm{o}} \\ r_{\mathrm{d}} = \sum_{j\neq i}^{I}\sum_{t=1}^{T}\left\|P_{ij,t}^{k+1} - P_{ij,t}^{k}\right\|_2 \leqslant \varepsilon_{\mathrm{d}} \end{cases} \tag{58}$$

where ε_{o} and ε_{d} represent small positive numbers that control the upper limits of the original and dual residuals, respectively.

The conventional ADMM uses a fixed penalty factor ρ, which, if not selected correctly, can lead to slower convergence or even non-convergence. Additionally, existing commercial solvers prolong the iteration time as the number of iterations increases. Therefore, improving the iteration process involves setting dynamic convergence accuracy and implementing a multi-segment hot-start strategy for the algorithm. This approach effectively mitigates the issue of prolonged single-round iteration times in later stages. Moreover, the penalty factor is appropriately adjusted in each segment of the iteration process to ensure optimal iteration speed.

For the multi-MGs day-ahead and intraday scheduling model, the solution process using the improved ADMM is outlined in Fig. 2.

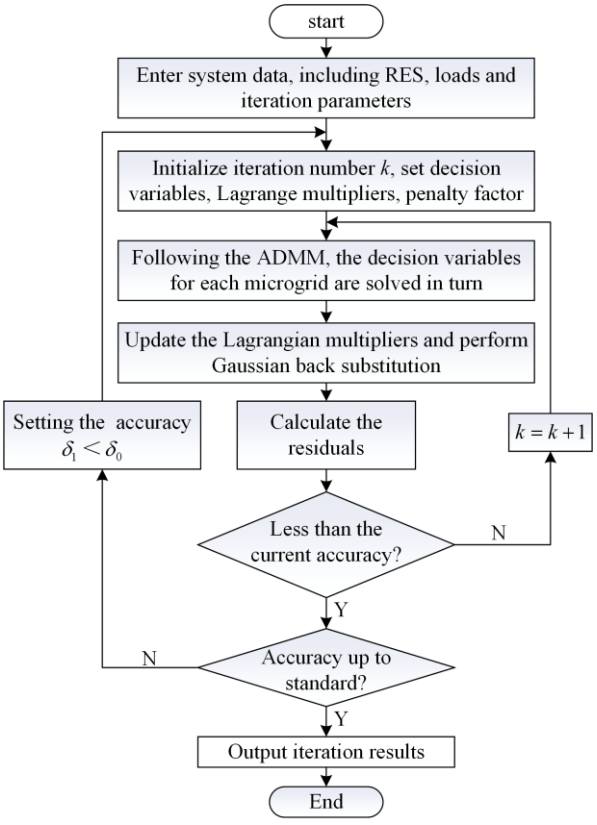

Fig. 2. Improved ADMM solution procedure.

C. Solving Profit Distribution Problem Based on NSGA-III Algorithm

NSGA-III introduces widely distributed reference points when solving a multi-objective optimization problem, such as (52), thereby mitigating local optima, and ensuring both convergence and population diversity to discover high-quality solutions across the Pareto front [30]. In (44), the decision variables π_{ij}^{P2P}, and define a product space of feasible domains that constitutes a convex bounded closed set. Additionally, the objective function is continuous with respect to these decision variables, indicating the existence of an immovable point in the product space, unchanged after negotiation, signifying the possibility of finding a Nash equilibrium point [31].

Consequently, the NSGA-III algorithm iteratively approximates or identifies the Nash equilibrium point, as illustrated in the following Fig.3.

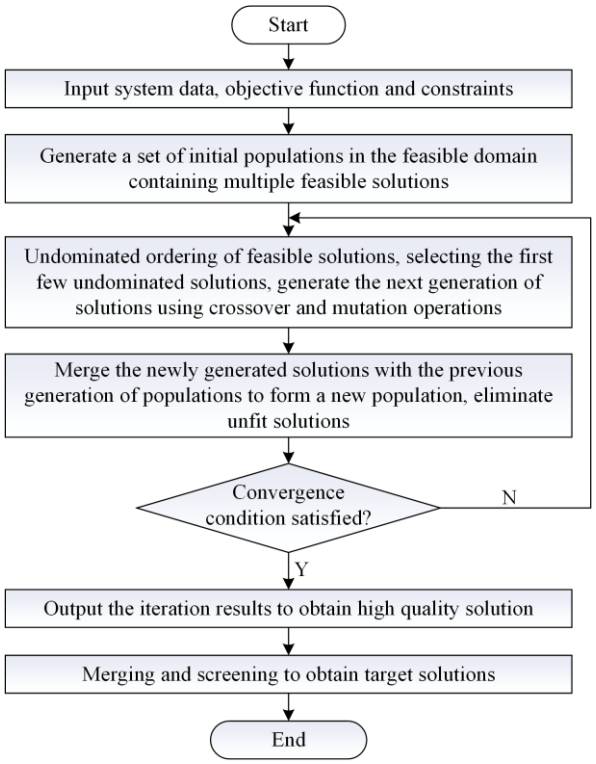

Fig. 3. Procedure of NSGA-III algorithm for solving profit distribution.

IV. Case Study

A. Case Data and Assumption

In this study, three MGs connected to a distribution network are analyzed to evaluate the cooperative operation between them in both day-ahead and intraday stages. Each MG incorporates rigid loads, flexible loads, GF, ESS, and RES. Specifically, MG1 contains CHP units, MG2 contains carbon capture power plants, and each MG differs in terms of DR implemented by time period and region, as well as localization of RES. RES and load data are derived from typical daily data for a

given region or generated using the load profile generator. The optimization algorithm is executed using Gurobi, invoked through Yalmip in Matlab, with a target convergence accuracy set to 0.1. For the NSGA-III algorithm, a population size of 60 is used, with the number of offspring set to 200.

To assess the impact of the cooperative operation model carbon emission reduction and efficiency improvement, three scenarios are established. The consideration of uncertainty is set in Scenario 3 by including prediction errors in the intraday scheduling stage, reflecting real-time fluctuations in RES and loads.

Scenario 1: Each MG operates independently, trading only with the upper grid.

Scenario 2: Each MG operates cooperatively, performing day-ahead optimal dispatch based on forecasted loads and RES with one-hour time interval.

Scenario 3: The MGs operate cooperatively, with intra-day scheduling based on day-ahead results. Prediction errors for RES and load at time t satisfy a normal distribution, with a mean of 0 and a standard deviation of 8% of the predicted value. The intraday scheduling is performed with a 15-min time interval.

Figure 4 displays the RES output of each MG, where DA/MG1 and ID/MG1 represent the day-ahead forecasted and intraday actual WT outputs for MG1. DA/MG2 and ID/MG2, along with DA/MG3 and ID/MG3, denote the day-ahead and intraday PV outputs for MG2 and MG3, respectively. The corresponding power and heat loads for each MG, forecasted day-ahead and intra-day, are depicted in Fig. 5.

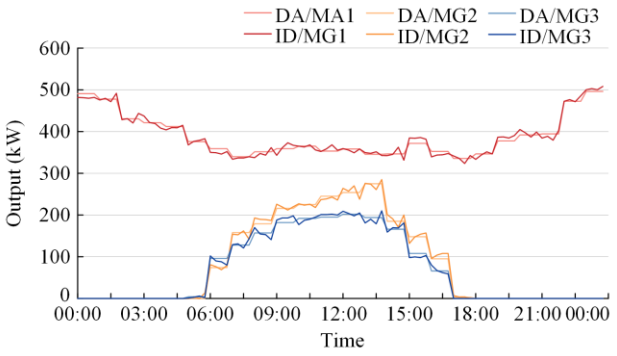

Fig. 4. RES output of each MG (DA: 1 hour interval; ID: 15 min interval).

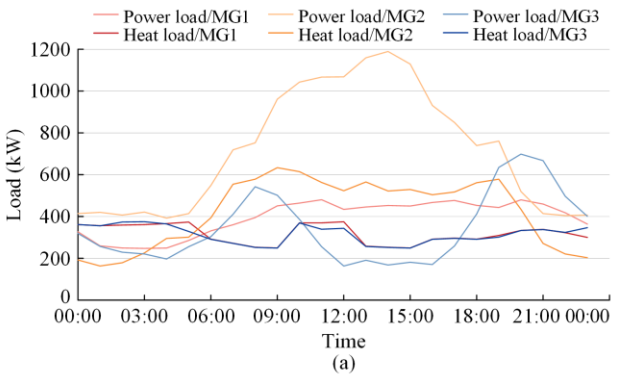

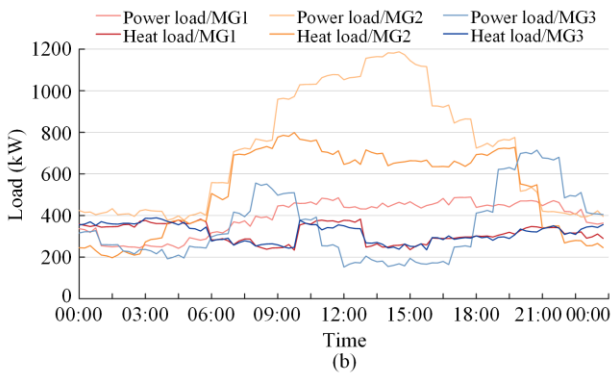

Fig. 5. Loads for each MG. (a) Predicted day-ahead values of loads for each MG (1 hour interval). (b) Actual intraday values of each MG load (15 min interval).

B. Analysis of Optimization Results for Multi-microgrids Cooperation

In scenarios 2 and 3, Fig. 6 shows the power interactions among MGs at time t, with positive values indicating inflow and negative values indicating outflow.

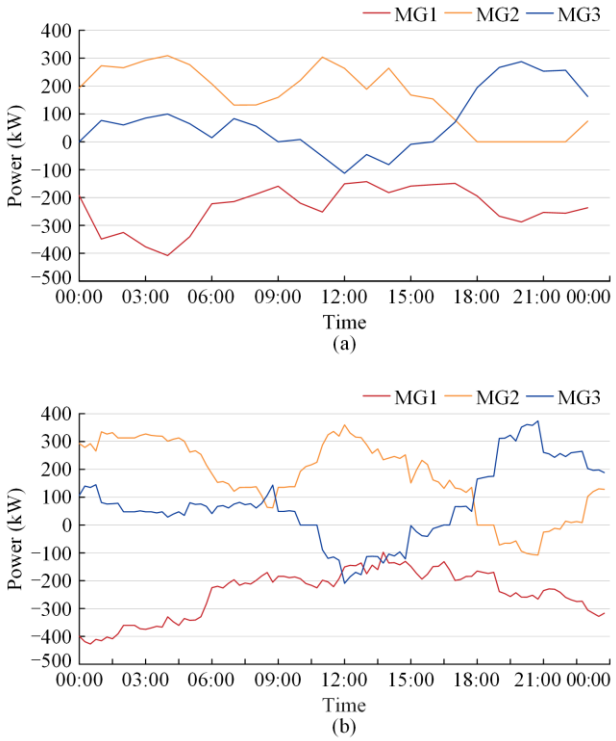

Fig. 6. Results of intraday power interactions. (a) Results of day-ahead power interactions (1 hour interval). (b) Results of intraday power interactions (15 min interval).

According to the figures, from 00:00 to 06:00, MG1 transfers more power to MG2 and MG3 due to its higher WT output is higher during this period, which meets the larger external demand for power brought by MG2 and MG3. In fact, the loads of all MG are at a low level during this period, and they can satisfy their loads to a relatively greater extent by relying on RES. During

07:00–09:00, the load of MG3 reaches its morning peak and accordingly, the received power increases. During 10:00–19:00, the important load of MG2 increases significantly and reaches the highest peak of the day, while the load of MG1 is more stable and the load of MG3 is low, allowing them to transfer excess power to MG2. From 20:00 to 24:00, MG3 reaches its evening peak load, and MG2's load begins to decrease. Despite no power interaction between MG2 and MG3 in the day-ahead stage, MG2 can still provide spare power to MG3 in the intraday stage, alleviating its load.

In general, results from both stages exhibit a similar overall trend with minor adjustments during certain periods, reflecting the flexible adjustment of each unit's output. These findings demonstrate that the cooperative operation of multi-MGs effectively manages the uncertainties of RES and load fluctuations while optimizing resource utilization.

Regarding MG2, Fig. 7 depicts the internal operation under scenarios 1, 2, and 3. In scenarios where power inflow into MG at the time t is positive and outflow is negative, ESS discharge is positive and charging is negative. P_{fix} and P_{dr} denote the power load conditions before and after DR, respectively. P_e represents electricity supplied to users post carbon capture, P_{PV} indicates PV output, and P_{ESS} illustrates the state of charge (charging and discharging). P_{out} and P_{ex} signify interactions of MG with the upper grid and other MGs, respectively.

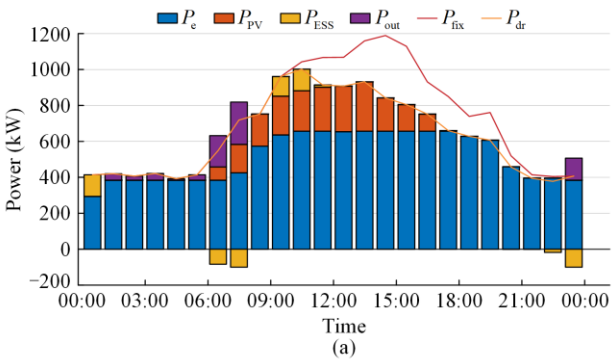

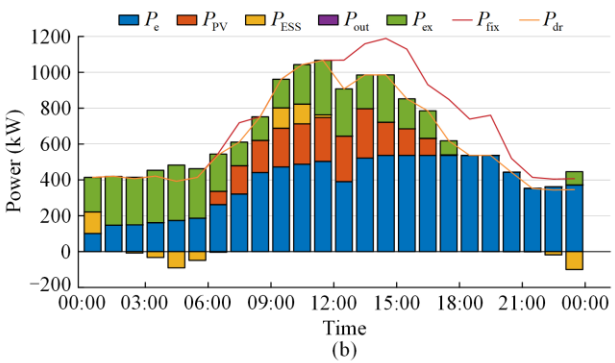

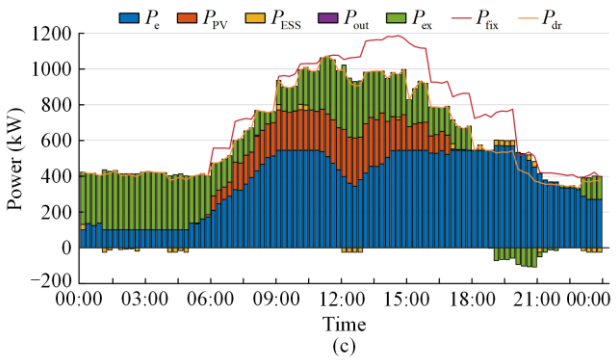

Fig. 7. MG2 operation results. (a) MG2 independent operation results (1 hour interval). (b) MG2 day-ahead operation results (1 hour interval). (c) MG2 intraday operation results (15 min interval).

During the peak load period of MG2, which coincides with the peak tariff times, IDR for load shedding is prohibited from 09:00 to 12:00. Therefore, it requires assistance from Class B IDR to respond earlier, from 06:00 to 08:00. Collaboration with other MGs enables MG2 to avoid purchasing power from the upper grid, thereby reducing pressure on the distribution network. Additionally, efficient power-sharing reduces the reliance on power plants, leveraging the rapid adjustment capabilities of CCSs. This flexibility allows for timely adjustments in power allocation and carbon capture needs, which is advantageous for intra-day stage adjustments and contributes to reduced carbon emissions. Comparing Figs. 7(a)–(c) horizontally, it is easy to find that MG2 inevitably purchases power from the upper grid when it operates independently, but since MG2 collaborates with other MGs, having less dependence, it no longer interacts with the upper grid, and the burden on the upper grid is reduced accordingly.

Table I presents the carbon emissions of each MG under scenarios 1, 2, and 3, along with the associated costs after carbon trading. The data illustrates that after power interaction, the carbon emissions are significantly reduced compared to independent operation. Moreover, after intraday optimization, there is a notable additional reduction in total carbon emissions across the MG group.

Among these, MG2 experienced the most significant decrease in carbon emissions due to reduced output from high carbon emission units facilitated by power interactions and the effective use of carbon capture technology during the intraday stage. This resulted in a greater decrease in carbon emissions for MG2 compared to the other MGs. MG3 has the largest percentage of decrease, primarily because it purchased less power from the upper grid, reducing its overall carbon footprint. Additionally, in the intraday stage, MG3 increased its utilization of RES consumption, which raised its carbon credit quota, offsetting the slightly higher carbon emissions observed in Scenario 3.

Specifically, the carbon emissions of each MG have been reduced by 6.23%, 13.41%, and 37.07%, respectively, and the total carbon emissions have been reduced

by 17.66%, this highlights that integrating intraday scheduling maximizes the performance of the units within each MG, effectively leveraging the synergy between RES and equipment, decreasing the output from high-carbon emission units, and thereby enhancing environmental benefits.

TABLE I
MG CARBON EMISSIONS

	Scenario 1		Scenario 2		Scenario 3		Carbon emission reduction rate (%)
	Carbon emission (kg)	Cost of carbon emissions (CNY)	Carbon emission (kg)	Cost of carbon emissions (CNY)	Carbon emission (kg)	Cost of carbon emissions (CNY)	
MG1	3592.67	1536.52	3372.64	1090.96	3368.89	1083.09	6.23
MG2	10 173.66	6201.26	8841.55	5534.61	8809.51	5522.49	13.41
MG3	4341.39	2514.72	2727.20	1335.35	2731.92	1320.57	37.07
Total	18 107.72	10 252.50	14 941.39	7960.91	14 910.33	7926.15	17.66

C. Analysis of Profit Distribution

Table II presents the operating costs under scenarios 1, 2, and 3. Following power interaction, the operating costs of each MG are decreased. Comparing scenarios 2 and 3 shows that cooperative operation helps mitigate RES fluctuations over short time frames, particularly when combined with Class B IDR to optimize the loads in time and to achieve the economic dispatch of MG.

TABLE II
OPERATING COSTS AND PROFIT DISTRIBUTION OF MG

	Scenario 1 cost	Scenario 2 cost	Scenario 3		Final cost
			Cost	Redis-tribution	
1	7605.9	6750.7	6595.5	885.3	5710.1
2	27 522.4	24 360.2	24 366.9	−707.3	25 074.3
3	9507.9	7180.7	7330.8	−178.5	7508.8
Total	44 636.2	38 291.6	38 293.2		38 293.2

After optimization, the MG group's operating cost decreased by 6342.99 CNY or 14.21%. Prior to profit distribution, MGs experienced profit increases of 1010.4 CNY, 3155.4 CNY, and 2177.1 CNY, respectively. Figure 7 highlights that MG 1 transmits the most power to the outside with the least profit improvement, indicating an imbalance. As a result, the iterative results of the profit distribution are given in Fig. 8, where the three coordinates denote the values adjusted by each MG in the process. The population distribution is concentrated in the figure, indicating satisfactory convergence achieved by the NSGA-III algorithm. Subsequently, the operating costs for each MG are 5710.1 CNY, 25074.3 CNY, and 7508.8 CNY, and the profit improvements of 1895.8 CNY, 2448.1 CNY, and 1999.1 CNY, respectively.

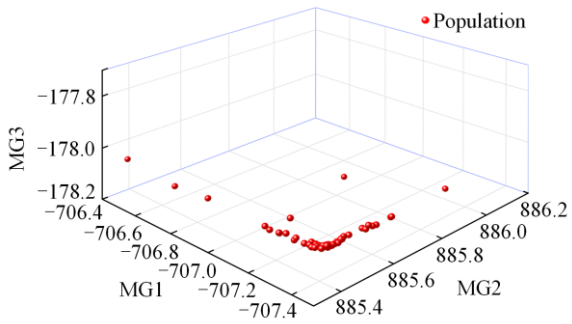

Fig. 8. Results of profit distribution.

Figure 9 presents the simulation outcomes of trading tariffs, demonstrating adherence to the peak-valley-flat tariff structure. This ensures grid exporting power during peak tariff periods is more profitable. The simulation also reflects changes on an hourly basis, aligning with electricity market operations. Overall, the trading simulation in this study supports reasonable profit distribution strategies.

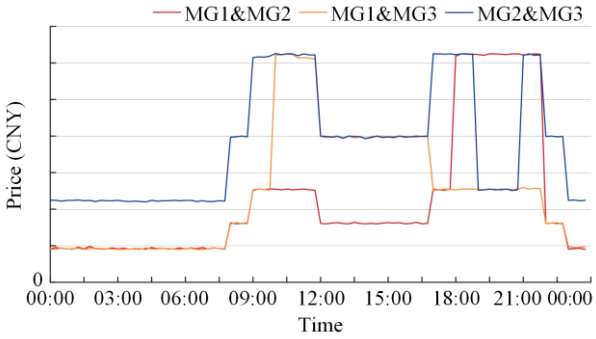

Fig. 9. Simulation results of trading tariffs between MGs (15 min interval).

MG1 exports power throughout the day and tends to receive more cooperative benefits. MG2 primarily receives power and has already achieved significant environmental benefits through cooperation and needs to compensate the other MG in redistribution; MG3 helps the other MG to consume RES and also transmits power externally during the day, whose profits need to be adjusted accordingly. Notably, MG1 has the largest amount of RES and has enough external power output to receive the most revenue. The redistribution of profit using generalized Nash equilibrium ensures the profit of each MG while taking into account fairness, improves the enthusiasm of MG to participate in power-sharing, and encourages MG and other operators to develop RES.

D. Convergence Analysis of Algorithms

1) Convergence Analysis of GBS-ADMM

Given that the multi-segment hot-start GBS-ADMM used in intraday scheduling in this paper is more rep-

resentative, the algorithm is taken as an example for the convergence analysis, and its residual convergence in the iterative process is shown in Fig. 10.

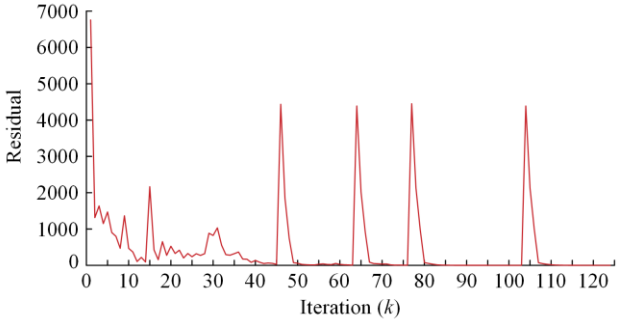

Fig. 10. The convergence of residuals in the intraday stage.

At the beginning of each iteration, the dual residual has large values, as indicated by the multiple spikes in the figure above. During the first and second iterations, there are pronounced fluctuations in the residuals. However, as the number of iterations increases, the results progressively improve, and the residuals quickly decrease to a lower level in subsequent rounds. After a total of 123 iterations, the convergence criterion is satisfied.

2) Convergence Analysis of NSGA-III Algorithm

The existing NSGA-II algorithm is widely utilized for solving multi-objective problems. Building on this foundation, the NSGA-III algorithm offers enhanced capabilities to explore different regions of the Pareto front, thereby improving the algorithm's convergence and the efficiency of the search for solutions. Using the three MG redistributed profits as coordinates and distinguishing the two algorithms by different colors, Fig. 11 illustrates the distribution of populations, that is, solutions, of the two algorithms across various iteration numbers. In comparison to Fig. 8, it is evident that as the number of iterations increases, the offspring population distribution of the NSGA-III algorithm becomes progressively more concentrated. By the end of the iteration process, the distribution range is significantly reduced, demonstrating better convergence performance.

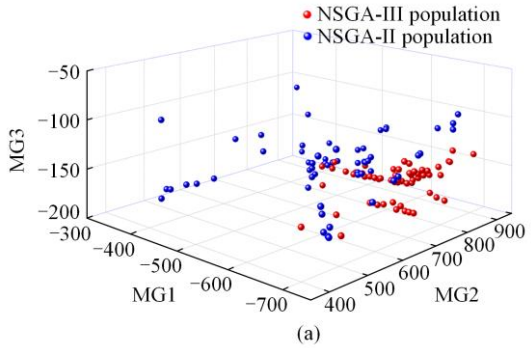

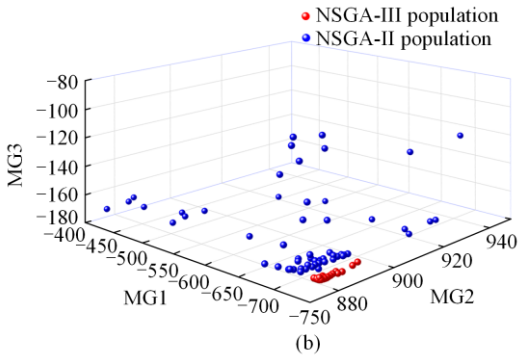

Fig. 11. Population distribution of different generations. (a) 75th generation population distribution. (b) 150th generation population distribution.

In addition, at the 75th iteration, the solution distributions for both the NSGA-III and NSGA-II algorithms are relatively wide. However, NSGA-III algorithm demonstrates a tendency to converge towards the Pareto front. By the 150th iteration, the solutions of both algorithms have converged to a narrower range, with NSGA-III's solutions being more concentrated and closer to the Pareto front. Overall, NSGA-III algorithm exhibits better distribution and diversity of the frontier solution set compared to NSGA-II, leading to superior performance in multi-objective optimization problems.

V. Conclusions

This study developed a day-ahead-intraday two-stage multi-MGs power-sharing model to explore the flexible scheduling potential of sources, storage, and demand within MGs, and to investigate the economic and low-carbon environmental benefits of cooperative operation among MG. The main conclusions are as follows:

1) Power interactions among MGs facilitate efficient consumption of RES. Mutual support among MGs can lower the use of high-carbon units within MGs, thereby decreasing carbon emissions and enhancing MG independence, which in turn reduces distribution network pressure.

2) Co-operation operations among MGs leverage the flexible scheduling capabilities of diverse devices to broaden MG's operational margins. This allows them to adapt to short-time scheduling challenges, smoothing out uncertainties stemming from source and demand fluctuations during actual operation.

3) The profit distribution method utilizing Nash equilibrium ensures that each MG benefits financially while maintaining fairness. This approach allocates profits according to each MG's contribution to the collective operation, thereby encouraging active participation in power-sharing, fostering the development of RES, and supporting a low-carbon economic framework.

The optimization algorithms tailored for various challenges have yielded effective results. The ADMM protects privacy by only requiring knowledge of the power transmitted between MGs. The addition of GBS and multi-stage hot-starting enhances convergence for complex systems. The NSGA-III algorithm avoids local optima and identifies high-quality solutions through parameter adjustments.

APPENDIX A

A. CHP Unit Constraints

A common pumped CHP unit is used as an example, where the CHP unit's power and heat feasible range is illustrated as ABCD in Fig. A1.

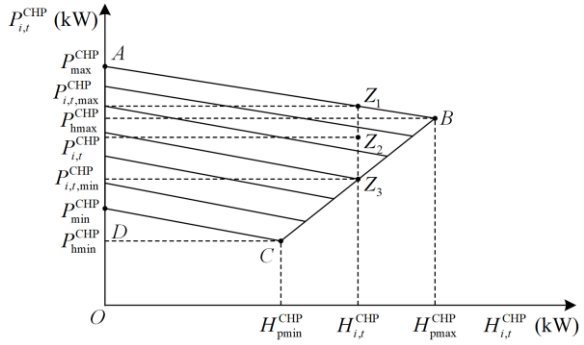

Fig. A1. Electro-thermal operating characteristics of the CHP units.

From Fig. A1, it can be observed that when the heat production power of the CHP unit is $H_{i,t}^{\mathrm{CHP}}$ (point Z2 in Fig. A1), its generating power interval is $\left[P_{i,t,\min}^{\mathrm{CHP}}, P_{i,t,\max}^{\mathrm{CHP}}\right]$ (points Z3 and Z1 in Fig. A1). The feasible domain of the CHP unit can be formulated as a linear constraint:

$$\begin{cases} P_{i,t}^{\mathrm{CHP}} \geqslant P_{\min}^{\mathrm{CHP}} + H_{i,t}^{\mathrm{CHP}} \dfrac{P_{\mathrm{hmin}}^{\mathrm{CHP}} - P_{\min}^{\mathrm{CHP}}}{H_{\mathrm{pmin}}^{\mathrm{CHP}}} \\ 0 \leqslant H_{i,t}^{\mathrm{CHP}} \leqslant H_{\mathrm{pmin}}^{\mathrm{CHP}} \\ P_{i,t}^{\mathrm{CHP}} \geqslant P_{\mathrm{hmin}}^{\mathrm{CHP}} + (H_{i,t}^{\mathrm{CHP}} - H_{\mathrm{pmin}}^{\mathrm{CHP}}) \dfrac{P_{\mathrm{hmax}}^{\mathrm{CHP}} - P_{\mathrm{hmin}}^{\mathrm{CHP}}}{H_{\mathrm{pmax}}^{\mathrm{CHP}} - H_{\mathrm{pmin}}^{\mathrm{CHP}}} \\ H_{\mathrm{pmin}}^{\mathrm{CHP}} \leqslant H_{i,t}^{\mathrm{CHP}} \leqslant H_{\mathrm{pmax}}^{\mathrm{CHP}} \\ P_{i,t}^{\mathrm{CHP}} \leqslant P_{\max}^{\mathrm{CHP}} + H_{i,t}^{\mathrm{CHP}} \dfrac{P_{\mathrm{hmax}}^{\mathrm{CHP}} - P_{\max}^{\mathrm{CHP}}}{H_{\mathrm{pmax}}^{\mathrm{CHP}}} \\ 0 \leqslant H_{i,t}^{\mathrm{CHP}} \leqslant H_{\mathrm{pmax}}^{\mathrm{CHP}} \end{cases} \tag{A1}$$

Since the above feasible domain is convex, the thermoelectric coupling factor $\omega_1 = \dfrac{P_{\mathrm{hmin}}^{\mathrm{CHP}} - P_{\min}^{\mathrm{CHP}}}{H_{\mathrm{pmin}}^{\mathrm{CHP}}}$ is chosen for minimum output, $\omega_2 = \dfrac{P_{\mathrm{hmax}}^{\mathrm{CHP}} - P_{\mathrm{hmin}}^{\mathrm{CHP}}}{H_{\mathrm{pmax}}^{\mathrm{CHP}} - H_{\mathrm{pmin}}^{\mathrm{CHP}}}$ is chosen for normal operation, and $\omega_3 = \dfrac{P_{\mathrm{hmax}}^{\mathrm{CHP}} - P_{\max}^{\mathrm{CHP}}}{H_{\mathrm{pmax}}^{\mathrm{CHP}}}$ is chosen for maximum output.

B. Linearization of MG Model

Equations (23) and (34) have multiple bilinear terms, which are linearized using the Big *M* method:

$$0 \leqslant P_{i,t}^{\mathrm{ch}} \leqslant x_{i,t}^{\mathrm{ch}} P_{i,\max}^{\mathrm{ch}} M \tag{A2}$$

$$0 \leqslant P_{i,t}^{\mathrm{disc}} \leqslant x_{i,t}^{\mathrm{disc}} P_{i,\max}^{\mathrm{disc}} M \tag{A3}$$

$$0 \leqslant P_{i,t}^{\mathrm{buy}} \leqslant x_{i,t}^{\mathrm{buy}} P_{i,\max}^{\mathrm{buy}} M \tag{A4}$$

$$0 \leqslant P_{i,t}^{\mathrm{sell}} \leqslant x_{i,t}^{\mathrm{sell}} P_{i,\max}^{\mathrm{sell}} M \tag{A5}$$

where *M* represents a large number.

ACKNOWLEDGMENT

Not applicable.

AUTHORS' CONTRIBUTIONS

Haiteng Han: funding acquisition and conceptualization. Yiteng Xu: writing-original draft, software and methodology. Chen Wu: writing-review and editing. Xiangchen Jiang, Shuyu Cao: formal analysis. Haixiang Zang: visualization. Sheng Chen: validation. Zhinong Wei: project administration. All authors read and approved the final manuscript.

FUNDING

This work is supported in part by the National Natural Science Foundation of China (No. 52307090), and in part by the Major Research Special Project on Science and Technology of Jiangxi Province (No. 20223AAE02011).

AVAILABILITY OF DATA AND MATERIALS

Please contact the corresponding author for data material request.

DECLARATIONS

Competing interests: The authors declare that they have no known competing financial interests or personal relationships that could have appeared to influence the work reported in this article.

AUTHORS' INFORMATION

Haiteng Han received the B.S. and Ph.D. degrees in Southeast University, Nanjing, China, in 2010 and 2019, respectively. From September 2016 to October 2017, he was a visiting scholar at the University of Tennessee, Knoxville, TN. He is currently a lecturer at Hohai University, Nanjing, China. His research interests include power system optimal dispatch, flexible resource planning and operation, and power electricity market.

Yiteng Xu received the B.S. degree in Yangzhou University, Yangzhou, China, in 2023. He is currently pursuing an M.Eng. degree at Hohai University, Nanjing, China. His research interests include power system optimal dispatch, microgrids planning and operation, and power electricity market.

Chen Wu received the B.S. and M.Eng. degrees in Southeast University, Nanjing, China, in 2010 and 2013, respectively. She is currently pursuing a Ph.D. degree at Hohai University, Nanjing, China. Her research interests include power system planning and operation, demand response, and power electricity market.

Xiangchen Jiang received the B.S. degree in Suzhou University of Science and Technology, Suzhou, China, in 2022. He is currently pursuing an M.Eng. degree at Hohai University, Nanjing, China. His research interests include smart grid, integrated energy system, and power electricity market.

Shuyu Cao received the B.S. degree in Nanjing Tech University, Nanjing, China, in 2024. He is currently pursuing an M.Eng. degree at Hohai University, Nanjing, China. His research interests include power system planning and operation, and power electricity market.

Haixiang Zang received the B.S. degree in electrical engineering from Nanjing Normal University in 2009, and the Ph.D. degree in electrical engineering from Southeast University in 2014. He is currently a professor with the School of Electrical and Power Engineering, Hohai University, Nanjing, China. His research interests include generation of renewable energy, and operation and control of power systems.

Sheng Chen received the B.S. and Ph.D. degrees from the College of Energy and Electrical Engineering, Hohai University, Nanjing, China, in 2014 and 2019, respectively. From January 2018 to January 2019, he was a visiting scholar with the Ohio State University, Columbus, OH, USA. He is currently a professor with the School of Electrical and Power Engineering, Hohai University. His research interests include integrated energy systems, operations research, and electricity markets.

Zhinong Wei received the B.S. degree from the Hefei University of Technology, Hefei, China, in 1984, the M.S. degree from Southeast University, Nanjing, China, in 1987, and the Ph.D. degree from Hohai University, Nanjing, in 2004. He is currently a professor of electrical engineering with the School of Electrical and Power Engineering, Hohai University. His research interests include integrated energy systems, power system state estimation, smart distribution systems, and integration of distributed generation into electric power systems.

REFERENCES

[1] K. Guerra, R. Gutiérrez-Alvarez, and O. J. Guerra *et al*., "Opportunities for low-carbon generation and storage technologies to decarbonise the future power system," *Applied Energy*, vol. 336, Apr. 2023.

[2] A. S. Satapathy, S. Mohanty, and A. Mohanty *et al*., "Emerging technologies, opportunities and challenges for microgrid stability and control," *Energy Reports*, vol. 11, pp. 3562-3580, Jun. 2024.

[3] M. Armioun, M. S. Nazar, and M. Shafie-khah *et al*., "Optimal scheduling of CCHP-based resilient energy distribution system considering active microgrids' multi-carrier energy transactions," *Applied Energy*, Vol. 350, Nov. 2023.

[4] Z. Wang and L. Mu. "Microgrid fault detection method coordinated with a sequence component current-based fault control strategy," *Protection and Control of Modern Power Systems*, vol. 9, no. 1, pp.81-93, Jan. 2024

[5] Y. Wang, J. Tang, and J. Si *et al*., "Power quality enhancement in islanded microgrids via closed-loop adaptive virtual impedance control," *Protection and Control of Modern Power Systems*, vol. 8, no. 1, pp.1-17, Jan. 2023

[6] L. Liu, X. Yao, and X. Qi *et al*., "Low-carbon economy configuration strategy of electro-thermal hybrid shared energy storage in multiple multi-energy microgrids considering power to gas and carbon capture system," *Journal of Cleaner Production*, vol. 428, Nov. 2023.

[7] X. Ma, Y. Wang, and J. Qin, "Generic model of a community-based microgrid integrating wind turbines, photovoltaics and CHP generations," *Applied Energy*, vol. 112, pp. 1475-1482, Dec. 2013.

[8] Z. Liu, Y. Chen, and R. Zhuo *et al*., "Energy storage capacity optimization for autonomy microgrid considering CHP and EV scheduling," *Applied Energy*, vol. 210, pp. 1113-1125, Jan. 2018.

[9] C. Essayeh, M. R. E. Fenni, and H. Dahmouni, "Optimization of energy exchange in microgrid networks: a coalition formation approach," *Protection and Control of Modern Power Systems*, vol. 4, no. 4, pp. 1-10, Oct. 2019.

[10] H. Onodera, R. Delage, and T. Nakata, "The role of regional renewable energy integration in electricity decarbonization—a case study of Japan," *Applied Energy*, vol. 363, Jun. 2024.

[11] H. Wu, M. Shahidehpour, and A. Alabdulwahab *et al.*, "Demand response exchange in the stochastic day-ahead scheduling with variable renewable generation," *IEEE Transactions on Sustainable Energy*, vol. 6, no. 2, pp. 516-525, Apr. 2015,

[12] Y. Zhang, K. Lin, and W. Deng *et al*. "A flexible voltage control strategy based on stage-division for microgrids," *Protection and Control of Modern Power Systems*, vol. 9, no. 3, pp. 60-69, May 2024.

[13] W. Gao and H. Lin, "Distributionally robust low-carbon optimal dispatch considering the risk of insufficient flexibi lity in distribution grids," *Power System Protection and C ontrol*, vol. 52, no.3, pp. 49-61, Aug. 2024. (in Chinese).

[14] A. Saxena and R. Shankar. "An interactive operating demand response approach for hybrid power systems integrating renewable energy sources," *Protection and Control of Modern Power Systems*, vol. 9, no. 3, pp. 174-194, May 2024.

[15] G. Sun, Z. Zhang, and Y. Zhou *et al*., "Bi-level model for integrated energy service providers in joint electricity and carbon P2P market," *Journal of Cleaner Production*, vol. 393, Mar. 2023.

[16] H. Han. S. Shen, and Z. Wei *et al*., "Security constrained distributed transaction model for multiple prosumers," *CSEE Journal of Power and Energy Systems*, vol. 10, no. 2, pp. 834-843, Mar. 2024.

[17] K. S. Alam, A. M. A. D. Kaif, and S. K. Das, "A blockchain-based optimal peer-to-peer energy trading framework for decentralized energy management with in a virtual power plant: Lab scale studies and large scale proposal," *Applied Energy*, vol. 365, Jul. 2024.

[18] Z. Ji, X. Liu, and D. Tang, "Game-theoretic applications for decision-making behavior on the energy demand side: a systematic review," *Protection and Control of Modern Power Systems*, vol. 9, no. 2, pp. 1-20, Mar. 2024.

[19] X. Yu, D. Pan, and Y. Zhou, "A Stackelberg game-based peer-to-peer energy trading market with energy management and pricing mechanism: a case study in Guangzhou," *Solar Energy*, vol. 270, Mar. 2024.

[20] S. Cui, S. Xu, and F. Hu *et al*., "A consortium blockchain-enabled double auction mechanism for peer-to-peer energy trading among prosumers," *Protection and Control of Modern Power Systems*, vol. 9, no. 3, pp. 82-97, May 2024.

[21] M. Nazari-Heris, B. Mohammadi-Ivatloo, and G. B. Gharehpetian *et al*., "Robust short-term scheduling of integrated heat and power microgrids," *IEEE Systems Journal*, vol. 13, no. 3, pp. 3295-3303, Sept. 2019.

[22] C. Kang, Z. Ji, and Q. Chen, "Review and prospects of flexible operation of carbon capture power plants," *Automation of Electric Power System*, vol. 36, no. 6, pp.1-10, Mar. 2012. (in Chinese).

[23] S. Ma, H. Liu, and Ni Wang *et al*., "Incentive-based integrated demand response with multi-energy time-varying carbon emission factors," *Applied Energy*, vol. 359, Apr. 2024.

[24] H. Cheng, T. Lu, and R. Hao *et al*., "Incentive-based demand response optimization method based on federated learning with a focus on user privacy protection," *Applied Energy*, vol. 358, Mar. 2024.

[25] C. Balasubramanian and R. L. R. Singh, "IOT based energy management in smart grid under price based demand response based on hybrid FHO-RERNN approach," *Applied Energy*, vol. 361, May 2024.

[26] Y. Ma, H. Wang, and F. Hong *et al*., "Modeling and optimization of combined heat and power with power-to-gas and carbon capture system in integrated energy system," *Energy*, vol. 236, Dec. 2021.

[27] X. Cheng, J. Lin, and F. Liu *et al*., "A coordinated frequency regulation and bidding method for wind-electrolysis joint systems participating within ancillary services markets," *IEEE Transactions on Sustainable Energy*, vol. 14, no. 3, pp. 1370-1384, Jul. 2023.

[28] B. He. "Modified alternating directions method of multipliers for convex optimization with three separable functions," *Operations Research Transactions*, vol. 19, no. 3, pp. 57-70, Mar. 2015.

[29] S. Cui, Y. Wang, and X. Liu *et al*., "Economic storage sharing framework: asymmetric bargaining-based energy cooperation," *IEEE Transactions on Industrial Informatics*, vol. 17, no. 11, pp. 7489-7500, Jan. 2021.

[30] Y. Wang, C. Chen, and Y. Tao *et al*., "A many-objective optimization of industrial environmental management using NSGA-III: a case of China's iron and steel industry," *Applied Energy*, vol. 242, pp. 46-56, May 2019.

[31] A. X. Jiang, K. Leyton-Brown, "A tutorial on the proof of the existence of Nash equilibria," University of British Columbia Technical Report TR-2007-25, 2009.

[32] S. Boyd, N. Parikh, and E. Chu *et al*., "Alternating direction method of multipliers," in *Distributed Optimization and Statistical Learning via the Alternating Direction Method of Multipliers*, 3th ed., Boston, USA: Now Foundations and Trends, 2011, pp. 11-22.